Spectroscopy of ^{16}F from the ^{16}O$(p,n)^{16}$F reaction at 99 and 135 MeV

A. Fazely, B. D. Anderson, M. Ahmad, A. R. Baldwin, A. M. Kalenda, R. J. McCarthy, J. W. Watson, and R. Madey
Department of Physics, Kent State University, Kent, Ohio 44242

W. Bertozzi, T. N. Buti, J. M. Finn, M. A. Kovash, and B. Pugh
Department of Physics and Laboratory for Nuclear Science, Massachusetts Institute of Technology, Cambridge, Massachusetts 02139

C. C. Foster
Indiana University Cyclotron Facility, Bloomington, Indiana 47401
(Received 19 November 1981)

We measured neutron energy spectra and extracted angular distributions for eleven separate transitions for the ^{16}O$(p,n)^{16}$F reaction at 99.1 and 135.2 MeV. Several new spin and parity assignments are obtained for states in ^{16}F by comparison of the excitation energy spectra with known analog states in ^{16}O and with a shell-model prediction and by analysis of the neutron angular distributions. The most strongly-excited states are two 2^- states at $E_x=0.40\pm0.05$ and 7.6 ± 0.1 MeV, a 4^- state at 6.37 ± 0.05 MeV, and two broad 1^- states at 9.4 ± 0.1 and 11.5 ± 0.1 MeV. These states are analogs of known 2^- ($M2$) states, a 4^- "stretched" state, and 1^- ($E1$) strength, respectively, in ^{16}O. Three weakly excited 1^+ states are observed at $E_x=3.75\pm0.05$, 4.65 ± 0.05, and 6.23 ± 0.05 MeV. These states are analogs of known 1^+ ($M1$) states in ^{16}O and directly indicate correlations in the ground state of ^{16}O. A weakly excited 4^- state is seen at 5.93 ± 0.05 MeV in good agreement with a 4^- state observed in ^{16}O (e,e') measurements. All of the most strongly excited states align (to within ±200 keV) with known $T=1$ analog states in ^{16}O for a common net displacement energy of 12.6 MeV. The (p,n) reaction at medium energies is shown to be an important spectroscopic tool.

NUCLEAR REACTIONS ^{16}O$(p,n)^{16}$F, $E=99.1$ and 135.2 MeV; measured neutron spectra in $\sim3°$ steps between 0° and 69°; extracted $\sigma(\theta)$ for eleven separate transitions to discrete states in ^{16}F. Compared excitation energies with analog states in ^{16}O and with a shell-model prediction. Deduced several new J^π assignments.

I. INTRODUCTION

Recent studies at the Indiana University Cyclotron Facility reveal that the (p,n) reaction at intermediate energies excites states predominantly via one-step processes. Goodman *et al.*[1] showed that zero-degree (p,n) reactions at 120 MeV are dominated by isovector spin-transfer transitions. These transitions lead to simple excitations of the residual nucleus and can be described well by impulse-approximation calculations.[2] The zero-degree (p,n) spectrum reported by Anderson *et al.*[3] for 160 MeV protons on ^{48}Ca agrees remarkably well with the shell-model prediction of 1^+ states by Gaarde *et al.*[4] Bertsch[5] described the basic features of this spectrum by a simple model of spin excitations. Watson *et al.*[6] showed recently that the most strongly excited states seen at larger angles in the ^{48}Ca(p,n) measurements are part of a particle-hole band and that the strongest transition is the largest spin member of this band. The measurements reported here further support the idea that direct-reaction mechanisms dominate (p,n) reactions at intermediate energies; consequently, the (p,n) reaction is an important spectroscopic tool. States strongly excited by one-step processes can be expected to be

dominated by simple structures amenable to theoretical descriptions.

We present here energy spectra and angular distributions for the ^{16}O$(p,n)^{16}$F reaction at 99.1 and 135.2 MeV. In order to obtain new spectroscopic information for states in ^{16}F, we compare the energy spectra of the excited states with known[7] states in ^{16}O, with inelastic electron[8–11] and proton[12,13] scattering measurements, and with a shell-model prediction.[14] The spins and parities of only a few states in ^{16}F were reported in the compilation of Ajzenberg-Selove.[7] From the agreement between the states observed in this experiment with known analog states in ^{16}O and with the predictions of a shell-model calculation,[14] we extract spectroscopic information for several new states in ^{16}F.

The comparison of states observed in these measurements with known states in ^{16}O is important also in the identification of $T=1$ states in the $A=16$ system. Recent observations[8,10,12,15] of $T=0$ and $T=1$, 4^- states in ^{16}O can be verified by comparison with the (p,n) spectra which can excite only $T=1$ states in ^{16}F. Especially interesting states identified to be $T=1$ in ^{16}O include the 2^- magnetic quadrupole state ($M2$) at $E_x=20.43$ MeV,[8,9] the strong 4^- state at $E_x=18.98$ MeV,[11,12,15] the weak 4^- state at 18.6 MeV,[11] and 1^+ ($M1$) states at $E_x=16.22$, 17.14, and 18.80 MeV.[10,13] Because $M1$ excitations are forbidden for a perfect closed-shell model of ^{16}O, the observation of these states provides a direct indication of ground-state correlations. It is advantageous to look for all of these $T=1$ states in ^{16}F where there is no background of $T=0$ states.

II. EXPERIMENTAL PROCEDURE

A. Experimental arrangement

We measured neutron time-of-flight (TOF) spectra from 99.1 and 135.2 MeV protons on a BeO target and from 135.2 MeV protons on a Be target. Shown schematically in Fig. 1 is the experimental arrangement associated with the beam-swinger system[16] at the Indiana University Cyclotron Facility (IUCF). For the measurements at 99.1 MeV, the neutron detectors were installed in two stations: one along the 0° line with respect to the undeflected proton beam at a distance of 68.1 m from the target, and the other along the 24° line with respect to the undeflected proton beam at a distance of 76.3 m from the target. Each NE-102 neutron detector was 1.02 m long by 0.102 m thick. Two 0.25 m high

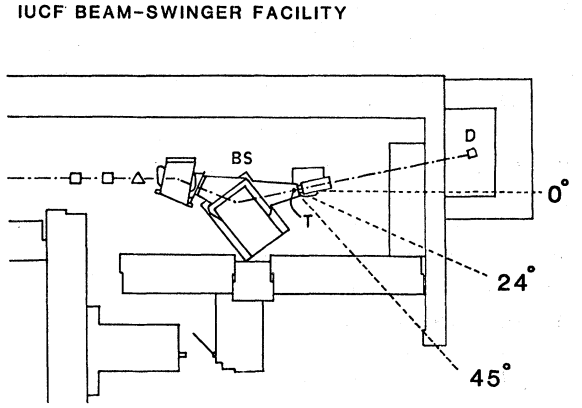

FIG. 1. Experimental arrangement associated with the beam-swinger facility at the IUCF. For measurements at 99.1 MeV, the neutron detectors were located in stations at 68.1 and 76.3 m from the target along the 0° and 24° lines, respectively; for measurements at 135.2 MeV, flights paths were 90.9, 90.8, and 73.4 m for the detectors at the 0°, 24°, and 45° lines, respectively.

neutron detectors with a combined frontal area of 0.52 m^2 were located in the 0° station; one 0.25 m high neutron detector and one 0.51 m high neutron detector with a total frontal area of 0.77 m^2 were located in the 24° station. For the measurements at 135.2 MeV, the neutron detectors were installed in three stations at 0°, 24°, and 45° with respect to the undeflected proton beam. The distances from the target to each detector system were 90.9, 90.8, and 74.4 m, respectively. The uncertainty in the flight paths is typically $\pm$0.2 m. Two 0.25 m high NE-102 neutron detectors with a combined frontal area of 0.52 m^2 were located in the 0° station; two 0.51 m high neutron detectors with a total frontal area of 1.03 m^2 were located in the 24° station; one 0.51 m high neutron detector, and one 1.02 m high neutron detector with a combined frontal area of 1.55 m^2 were located in the 45° station. An Amperex XP2041 photomultiplier tube (PMT) with a diameter of 0.127 m was attached to each end of each detector via a tapered plexiglas light pipe. The performance of these large-volume neutron detectors was reported previously by Madey *et al.*[17] and is discussed briefly for this experiment in Sec. III A. Since the beam swinger is capable of deflecting the incident proton beam through an angle of up to 24.5°, we were able to detect scattered neutrons from 0° to 24.5° at the 0° station, from 24° to 48.5° at the 24° station, and out to 69.5° at the 45° station. Charged particles produced by nuclear reactions in the target were vetoed by thin (0.635, 0.953, or 1.27 cm thick) plastic NE-102 or NE-114 scintillation

counters placed immediately in front of the neutron detectors. These anticoincidence counters plus similar thin plastic scintillator counters placed above the neutron detectors vetoed cosmic rays.

In order to be able to reliably calculate the neutron detection efficiency, it was necessary to determine the pulse-height (PH) response of each counter. For the first experiment with 99.1 MeV incident protons, the PH response was determined in a separate measurement with 160 MeV protons elastically scattered from a ^{40}Ca target. The energy of the protons arriving at the detectors was determined from the scattering energy by subtracting the calculated energy losses of the protons in the exit foil of the scattering chamber, the air, the wall of the detector station, and the anticoincidence counter. The calculated proton energy was 99 ± 2 MeV. A separate pulse-height (PH) calibration was performed with a ^{228}Th radioactive gamma source, which emits a 2.61 MeV gamma ray. A fast amplifier and precision attenuators were used to obtain a PH calibration curve which extrapolated to be in agreement with the proton calibration to within 3%. For the 135 MeV experiment, PH calibrations were performed with the ^{228}Th gamma-ray source and checked by verifying that the 0° cross section for the ^{12}C$(p,n)^{12}$N (g.s) reaction was consistent with our earlier measurements[18] at 120 and 160 MeV. This check is estimated to be accurate to $\pm10\%$.

B. Electronics

The data-acquisition system included a Tennecomp TP-5000 (PDP11/15) computer system, three 12-bit analog-to-digital converters (ADC's), commercially available electronic modules, and special electronic modules[19] developed at Kent State University to provide increased count-rate and dynamic-range capabilities for fast neutron time-of-flight (TOF) measurements. Figure 2 shows schematically the major elements of the data-acquisition system.

The anode signal from each end of each counter was split by a linear fan-out module (LFM) which produced two signals (nearly) identical to the original one. One of the LFM signals went to a constant-fraction discriminator (CFD) in order to obtain an accurate timing signal. The output from the CFD at each end of each counter served as inputs to an analog mean-timer (MT) circuit developed by Baldwin and Madey.[20] The output of the MT produced a start signal to a time-to-amplitude converter (TAC) which in turn provided

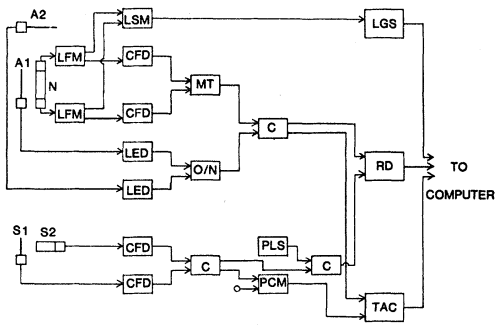

FIG. 2. Schematic diagram of the electronics and data-acquisition system. Key to abbreviations: LFM=linear fan-out; CFD=constant-fraction discriminator; LED=leading-edge discriminator; LSM=linear-summing module; MT=mean timer; O/N=or-nor logic unit; C=coincidence unit; PCM=phase-compensator module; RD=router-driver logic unit; LGS=linear gate and stretcher; and TAC=time-to-amplitude converter.

the neutron time-of-flight spectrum. The stop signal for the TAC was derived from the radio frequency signal of the cyclotron. The other anode-signal outputs of the LFM's from both ends of each counter were summed and integrated by a linear summing module (LSM) to provide a pulse-height measurement. Signals from different counters were identified by a tag word provided to a separate ADC.

A phase-compensation module[21] was used to eliminate drift between the time of arrival of a beam burst on the target and the stop signal derived from the cyclotron radio-frequency signal. Detection in a fast plastic scintillator of protons elastically scattered in the target provided the nesessary timing information to the phase-compensation circuit.

III. DATA REDUCTION

The recorded data were analyzed off-line at Kent State University. After choosing an appropriate (software) pulse-height threshold, all the magnetic tapes were reread in order to combine different runs at the same scattering angle. The neutron time-of-flight spectra thus obtained were converted to energy spectra and were analyzed to obtain cross sections for specific transitions as described below.

A. Energy resolution

The energy resolutions for states observed in ^{16}F were approximately 260 and 310 keV for the in-

cident proton energies of 99.1 and 135.2 MeV, respectively. The fractional energy resolution $\Delta T/T$ for a neutron of kinetic energy T can be calculated from the expression:

$$\Delta T/T=[\gamma(\gamma+1)](\Delta t/t)\ , \quad (1)$$

where t is the neutron time-of-flight, Δt is the overall time resolution, and $\gamma=1+T/M$. The sources contributing to the overall time resolution are (i) the intrinsic time resolution of the neutron detector, (ii) the beam-burst width from the cyclotron, (iii) the time spread in the neutrons arising from the finite target thickness, (iv) the time spread resulting from the finite thickness of the counter, and (v) the time spread in the neutrons from the energy spread of the beam. The intrinsic time resolution of the neutron detectors was obtained experimentally with a series of cosmic-ray measurements at Kent State University. The beam-burst widths were measured with a fast-plastic scintillator which detected protons elastically scattered from the target. The contributions of the separate sources in each experiment are presented in Table I. The overall estimated time spreads with a 47.4 mg/cm^2 ^{9}Be^{16}O target at 99.1 and 135.2 MeV proton beam energies are 1150 and 820 picoseconds, respectively. Note that these overall dispersions are not the quadrature combination of the individual sources (since the target and detector contributions are not Gaussian in shape), but a proper numerical convolution of the contributing sources. The calculated time resolutions are in good agreement with the overall observed time resolutions of 1000 and 830 picoseconds given in Table I.

For $\Delta t=1000$ picoseconds in the first experiment, we obtained $\Delta T=260$ keV for the 80 MeV neutrons from the ^{16}O(p,n)^{16}F reaction; for $\Delta t=830$ picoseconds in the second experiment, we obtained $\Delta T=310$ keV for 110 MeV neutrons from the ^{16}O(p,n)^{16}F reaction. For the detectors in the third station at 74.4 m in the second experiment, the value of ΔT was 380 keV.

B. Conversion to energy spectra

The ^{9}Be(p,n)^{9}B ground-state peak in each time-of-flight spectrum from the BeO target served as a calibration point for determining the absolute neutron kinetic energies. Figure 3 is a time-of-flight spectrum at 24° from the ^{9}Be^{16}O target. The ground state (p,n) Q values on ^{9}Be and ^{16}O are -1.85 and -16.21 MeV, respectively; thus, the low-lying states excited in ^{9}B are well separated in the time-of-flight spectra from the states excited in ^{16}F, as seen in Fig. 3. Data for the ^{9}Be(p,n)^{9}B reaction at 135 MeV indicate that high-lying states of ^{9}B are seen for excitation energies of about 14.1, 14.65, 16.96, and 17.71 MeV. These states will appear in ^{16}F excitation energy spectra at excitation energies of about 0.40, 0.70, 2.6, and 3.35 MeV. In our 135.2 MeV experiment, we identified these states in the ^{9}Be(p,n)^{9}B spectra and performed a channel-by-channel subtraction of ^{9}Be(p,n)^{9}B spectra from ^{9}Be^{16}O(p,n) spectra. The neutron TOF spectra were converted to excitation-energy spectra, some of which are shown in Figs. 4 and 5 for the 99.1 and 135.2 MeV experiments, respectively.

C. Cross sections

The laboratory differential cross sections were obtained from the usual expression

$$\sigma(\theta)=N/[I(\rho x N_0/A)\Delta\Omega\epsilon Tl]\ , \quad (2)$$

where N is the number of counts above background in the peak of interest, I is the time-integrated pro-

TABLE I. Time dispersions (in picoseconds) from various sources.

Beam energy (MeV)		99.1	135.2
Flight path (m) to detector station at 24°		76.3	90.8
Intrinsic		368	300
Beam energy spread (=0.1%)		327	338
Beam burst width		572	350
Target (47.4±0.8 mg/cm^2 ^{9}Be^{16}O)		967	596
Detector thickness		657	560
Overall	Calculated	1150	820
	Observed	1000	830

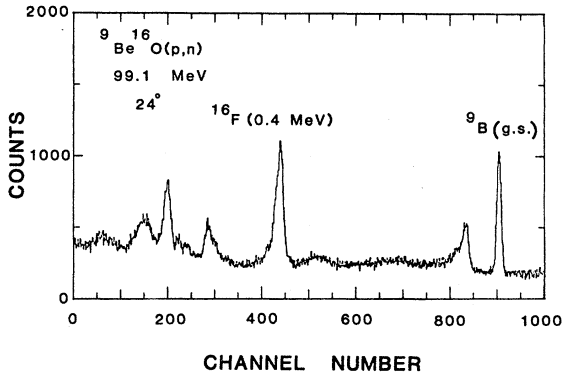

FIG. 3. Neutron time-of-flight spectrum at 24° from 99.1 MeV protons on beryllium oxide ($^9Be^{16}O$).

ton flux through the target, ρx is the thickness of the target in g/cm^2, N_0 is Avogadro's number, A is the mass number of the target nucleus, $\Delta\Omega$ is the solid angle (in steradians) subtended by the neutron

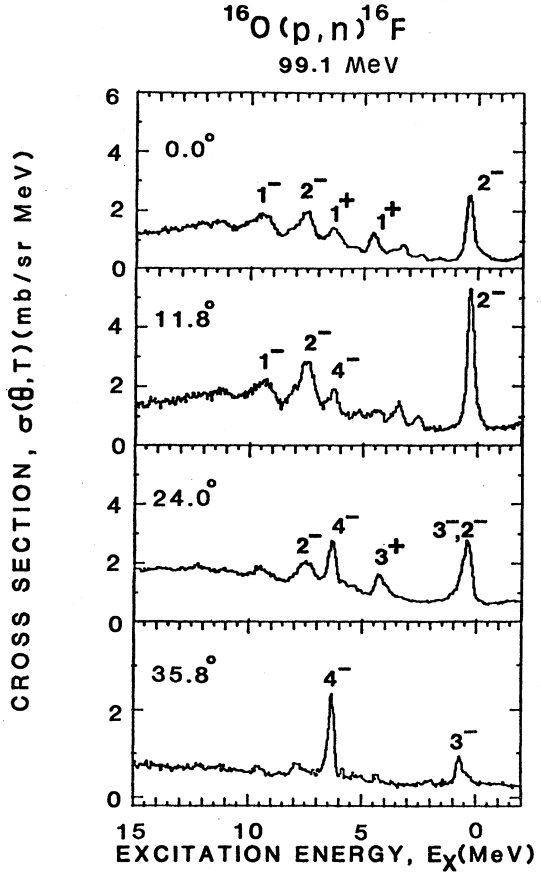

FIG. 4. Excitation energy spectra for the $^{16}O(p,n)^{16}F$ reaction at 99.1 MeV. Note that $^9Be(p,n)^9B$ contaminant peaks have not been subtracted. Spin and parity assignments for most of the states identified in this work are shown. See text.

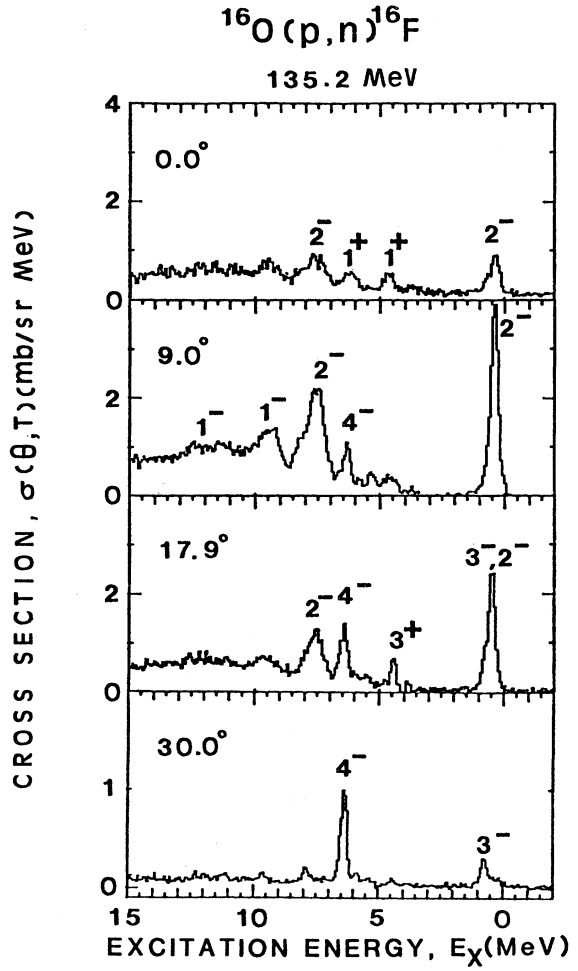

FIG. 5. Excitation energy spectra for the $^{16}O(p,n)^{16}F$ reaction at 135.2 MeV. Spin and parity assignments for most of the states identified in this work are shown. See text.

detector, T is the fraction of the neutrons transmitted through the air and other intervening material to the neutron detector, ϵ is the neutron detection efficiency, and l is the livetime of the data-acquisition system.

The number of counts under a particular peak was determined by peak fitting. A computer code based on the original code of Bevington[22] was used to fit a particular region of the time-of-flight spectrum with an appropriate number of Gaussian line shapes above a polynomial background. The fitting program performs a least-squares fit by a combined grid search and linearization technique.

The neutron detector efficiencies were calculated with the Monte Carlo code of Cecil *et al.*[23] This code was tested by comparison with several pub-

lished neutron detector efficiency measurements including a comparison[18] of measured ^{12}C(p,n)^{12}N and ^{12}C(p,p')$^{12}C^*$ analog transition cross sections at 62 and 120 MeV. Cecil *et al.* estimate an uncertainty of a few percent in the calculated efficiencies for well-determined thresholds; in addition, there is a further uncertainty in the efficiency resulting from an uncertainty in the threshold setting used to analyze the data. For the 99.1 MeV experiment, the uncertainty in the 40 MeV equivalent-electron (MeV *ee*) energy threshold was estimated to be $\pm 3\%$ and results in an additional $\pm 9\%$ uncertainty in the calculated efficiency. This relatively high threshold was needed to eliminate overlap in the time-of-flight spectra of neutrons from adjacent beam bursts. The 9% uncertainty arises because the energies of the neutrons, which are between 70 and 80 MeV, are less than twice the pulse-height threshold energy of about 50 MeV for the recoil protons. In this region near threshold, the efficiencies increase sharply with neutron energy and are very sensitive to threshold uncertainties. For the 135 MeV experiment, neutron detector thresholds of 70 MeV *ee* were required in order to eliminate overlap of the high excitation-energy part of the continuum from the previous beam burst with the low-lying states of ^{9}B and ^{16}F; however, because the continuum appeared small and structureless, the data were analyzed at thresholds of about 50 MeV *ee* in order to improve the statistics (by increasing the detector efficiency). For the 115 MeV neutrons of interest from the ^{16}O(p,n)^{16}F reaction, a 3% uncertainty in the threshold results in an additional uncertainty in the calculated efficiencies of about 4%.

The solid angle $\Delta\Omega$ for the large rectangular detectors was determined from the exact expression of Crawford.[24] The livetime correction l, which represents the fraction of the time that the data-acquisition system was not blocked to the incoming data, was measured as the ratio between the number of events analyzed by the system to the total number of events sent to the computer. The measured livetimes varied between 87 and 94 percent. The neutron attenuation correction is the product of the exponential attenuation factors[25] for neutrons traversing the exit foil, the air, the detector station wall, and the charged-particle veto counters. Neutron transmissions were 81 to 82 percent for the 99.1 MeV experiment and varied from 78 to 84 percent for the 135.2 MeV experiment. The calculated detector efficiencies varied from 2.2 to 2.3 percent for the 99.1 MeV experiment and from 2.4 to 2.8 percent for 135.2 MeV experiment.

The overall scale uncertainties for the 99.1 and 135.2 MeV experiments are estimated to be 11.2 and 8.3 percent, respectively. The separate contributions leading to these net uncertainties are listed in Table II.

IV. RESULTS

Excitation energy spectra for the 99.1 and 135.2 MeV data are shown in Figs. 4 and 5. The 135.2 MeV spectra include a channel-by-channel ^{9}Be(p,n)^{9}B subtraction as described in Sec. III. In the 99.1 MeV spectra, the contamination of the ^{9}Be(p,n) reaction has not been removed. These excitation energy spectra from both the 99.1 and 135.2 MeV experiments reveal distinct peaks corresponding to at least eleven different excited states in ^{16}F.

Extracted angular distributions for the resolved excited states of ^{16}F are shown in Figs. 6 and 7 for the 99.1 and 135.2 MeV measurements, respectively. The area under each peak was extracted by fitting the time-of-flight spectrum with Gaussian functions on a polynominal background (see Sec. III C above). The error bars include statistical uncertainties plus a contribution for the accuracy of the fitting procedure obtained from the error matrix of the fitting program.[22]

V. ANALYSIS

In order to determine the spin and parities of the final states in ^{16}F, we compared excitation energies with analog states in ^{16}O, deduced l transfers from the measured angular distributions, and compared the measurements with a shell-model prediction. In the following sections, we will discuss and analyze

TABLE II. Scale uncertainties (%).

	99.1 MeV	135.2 MeV
Beam integration	$\lesssim 2$	$\lesssim 2$
Target thickness	1.7	1.7
Detector efficiency	10	6
Neutron attenuation	~ 4	~ 5
Solid angle	$\lesssim 0.5$	$\lesssim 0.5$
Livetime	~ 1	~ 1
Overall	11.2	8.3

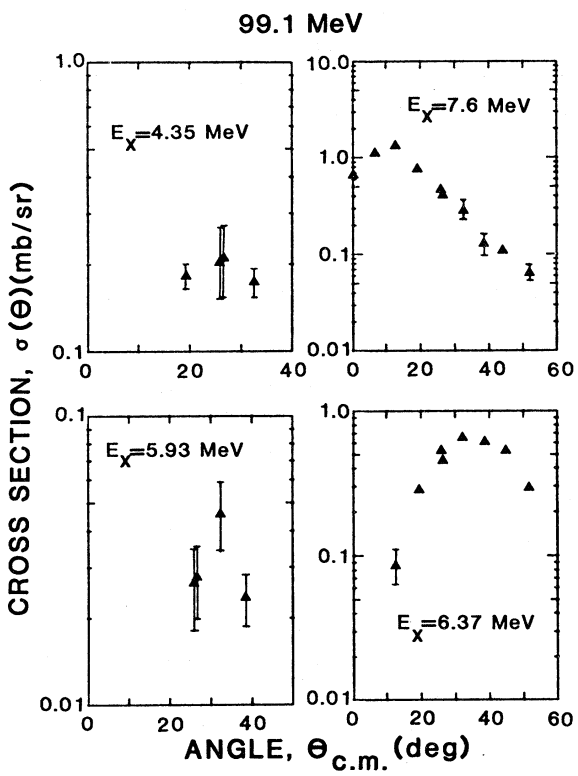

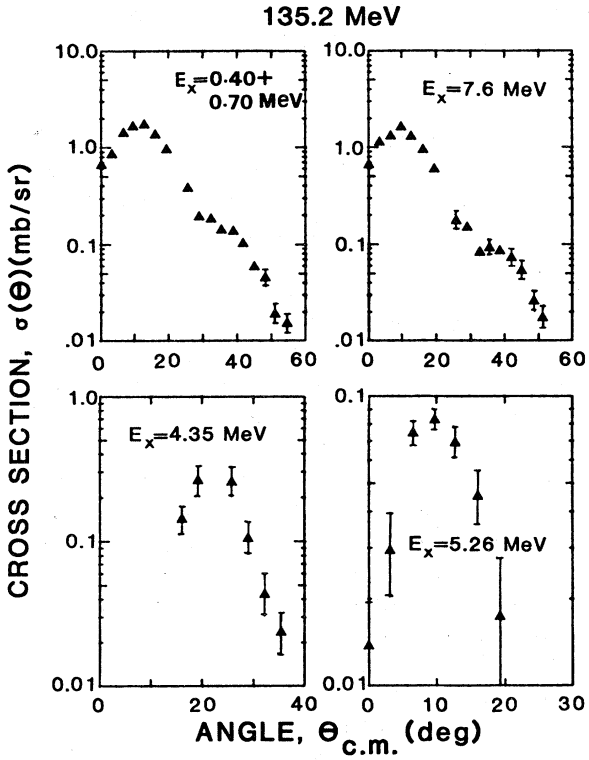

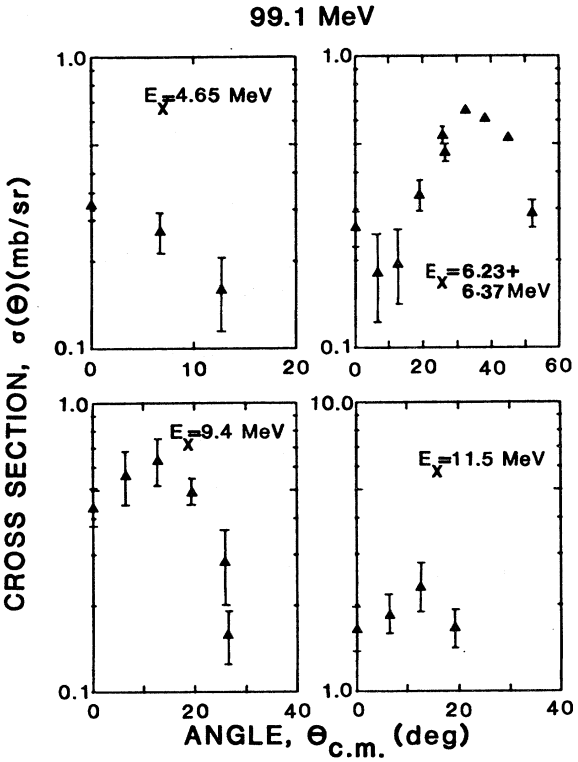

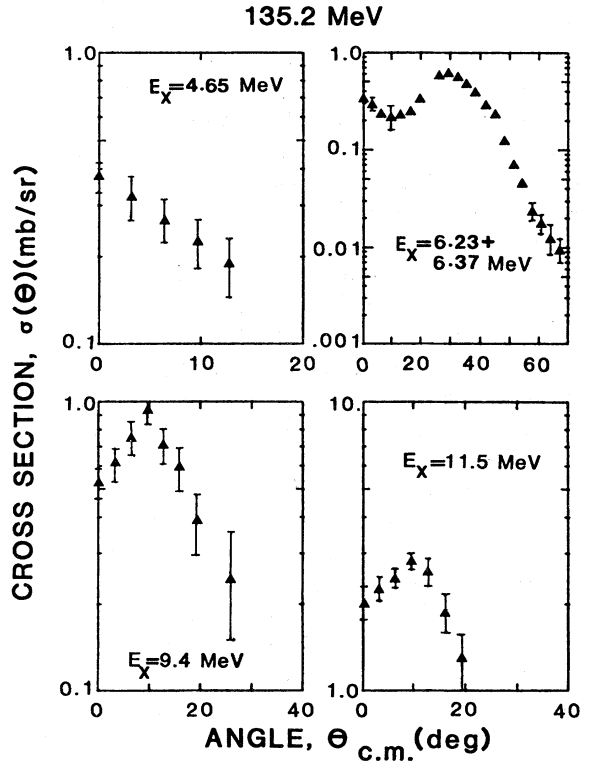

FIG. 6. Angular distributions for the resolved excited states of ^{16}F at 99.1 MeV.

FIG. 7. Angular distributions for the resolved excited states of ^{16}F at 135.2 MeV.

separately each of the several strong transitions observed in Figs. 4 and 5; before we begin to discuss individual transitions, however, we note that the angular distributions presented in Figs. 6 and 7 all seem to peak at regular intervals. For the 99 MeV results presented in Fig. 6, the angular distributions all peak near 0°, 12°, 24°, or 36°. For the 135 MeV results presented in Fig. 7, the angular distributions all peak near 0°, 10°, 20°, or 30°. These regular angular intervals would suggest that these peaks correspond to l transfers of 0, 1, 2, and 3 units of angular momentum. We will examine this possibility separately for each transition of interest by comparing the measured angular distribution with the distorted-wave impulse-approximation (DWIA) calculation. We choose to start with the state observed at $E_x=6.37$ MeV, which singularly dominates the wide-angle spectra. This state is logically a 4^- state whose analog is well known in ^{16}O and is believed to have a particularly simple nuclear structure. This state should provide a clear starting point for comparing $T=1$ analog states in ^{16}F and ^{16}O.

A. The 6.37 MeV State

At the wide angles, a strong transition to a state at $E_x=6.37$ MeV in ^{16}F is seen to dominate. The angular distribution is peaked near 36° and 30° at 99 and 135 MeV, respectively, suggesting $\Delta l=3$. Since the ground state of ^{16}F is[7] (apparently) a 0^- state whose analog is observed in ^{16}O at $E_x=12.80$ MeV, we would expect to see the analog of this 6.37 MeV state near $12.80+6.37=19.17$ MeV in ^{16}O. This excitation energy is within 200 keV of a 4^-, $T=1$ state seen in ^{16}O via the (e,e') and (p,p') reactions.[8,12] Figure 8 compares our ^{16}O(p,n) energy spectrum at 35.8° and 135 MeV with the ^{16}O(p,p') spectrum of Henderson *et al.*[12] at 35° and 135 MeV. The energy scales were adjusted to be the same, but the origins were offset to align the ^{16}F ground state with its analog in ^{16}O. The spectra show the good alignment of the 6.37 MeV state in ^{16}F with the $T=1$, 4^- state at 18.98 MeV in ^{16}O. The two strong $T=0$, 4^- states seen in ^{16}O are clearly missing in the (p,n) spectrum as expected. (Note that although these three 4^- states are known[15] to be isospin mixed in ^{16}O, this mixing will not occur in ^{16}F where no $T=0$ states are available to mix with the $T=1$ state.)

The excitation of this state is especially interesting because it is believed to be a so-called "stretched" state with a predominant configuration ($\pi d_{5/2}, \nu p_{3/2}^{-1}$). Since we expect that the excitation

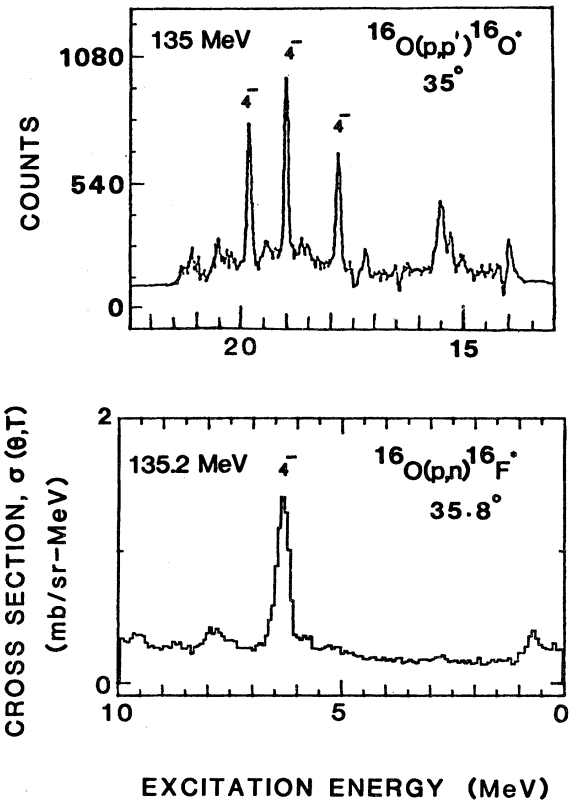

FIG. 8. Comparison of the excitation energy spectrum at 35.8° for the ^{16}O(p,n)^{16}F reaction at 135.2 MeV with the excitation energy spectrum of Henderson *et al.* (Ref. 12) at 35° for the ^{16}O(p,p')^{16}O reaction at 135 MeV.

of this state via the (p,n) or (p,p') reactions should proceed primarily through the isovector tensor term of the nucleon-nucleon effective interaction, the study of this transition should test our knowledge of the strength and momentum transfer dependence of that term. The momentum transfer dependence of the differential cross section for this transition is compared in Fig. 9 to that of Henderson *et al.* for the analogous (p,p') reaction. The (p,p') cross sections are multiplied by two to account for the ratio of the isospin Clebsch-Gordan coefficients for the (p,n) and (p,p') excitation of a $T=1$ state from a $T=0$ target.[18] Shown also are the results of distorted-wave impulse-approximation (DWIA) calculations for these transitions performed by us with the code DWBA70,[26] which includes a recent modification of the relativistic kinematics. The DWIA calculations use harmonic-oscillator bound-state wave functions with an oscillator parameter $b=1.73$ for the particle-hole states, the NN t-matrix interaction of Love and Franey[27] at 140 MeV, and

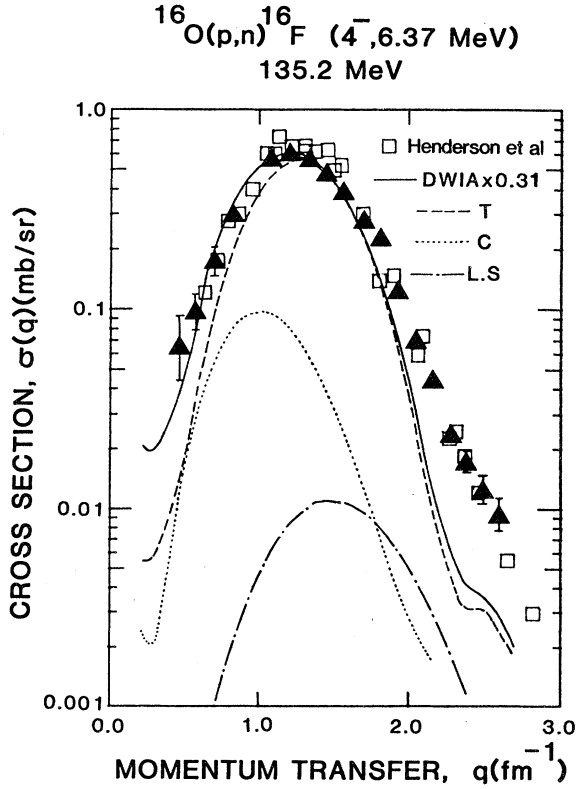

FIG. 9. The differential cross section versus the momentum transfer for the transition to the 4^- state in the reaction $^{16}O(p,n)^{16}F$ (6.37 MeV). Shown for comparison are the (p,p') data of Henderson *et al.* (Ref. 12) which are multiplied by two to account for the isospin Clebsch-Gordan coefficients. Shown also are the results of DWIA calculations for this transition to a stretched particle-hole $(\pi d_{5/2},\nu p_{3/2}^{-1})$ configuration. The DWIA calculation uses the effective interaction of Love and Franey (Ref. 27) at 140 MeV and the optical model parameters of Comfort and Karp (Ref. 28).

the optical model parameters determined by Comfort and Karp[28] for 135 MeV protons elastically scattered from ^{12}C. Note that this transition is dominated by the isovector tensor term in the effective interaction as shown in Fig. 9. We determined the ratios of the experimental cross sections to the theoretical calculations to be 0.33 and 0.31 for the (p,p') and (p,n) transitions, respectively. If we take the normalization required for the (e,e') excitation of this state, viz., 0.44 (Ref. 8) to be a measure of the renormalization required for the nuclear structure, then the (p,n) and (p,p') results may indicate some deficiency in the DWIA description of the proton-induced reactions; for example, a small variation of the isovector tensor interaction would bring the results into better agreement with the electron scattering results.

Because of the clear identification of the 6.37 MeV state as the "parent" of the 18.98 MeV state in ^{16}O, and because we do not reliably see the ground state of ^{16}F excited in these measurements, we will henceforth take the observed displacement between the 4^- states as the net displacement energy between states in ^{16}F and their analogs in ^{16}O. Thus we assume a net displacement energy of $18.98-6.37=12.61$ MeV. Clearly, different states will have slightly different displacement energies resulting primarily from differences in the distribution of the extra charge in ^{16}F.

B. The 0.40 and 7.6 MeV states

Besides the 4^- state at 6.37 MeV, the most strongly excited states observed in these measurements are transitions to states at $E_x=0.40$ and 7.6 MeV. Both of these states have angular distributions peaked near 10°, suggesting $\Delta l=1$. These transitions are plausibly 2^- states whose analogs are known[7] at appropriate excitation energies in ^{16}O. Backward-angle electron scattering measurements (which predominantly excite $T=1$ states also) strongly excite 2^- states in ^{16}O at 12.97 and 20.43 MeV.[8,9] [In fact, the general features of the electron scattering measurements are similar to those seen in the (p,n) energy spectra reported here.] These excitation energies in ^{16}O agree to better than 200 keV with the excitation energies for the states at $E_x=0.40$ and 7.6 MeV in ^{16}F using the net displacement energy (viz., 12.6 MeV) observed for the $T=1$, 4^- state.

The excitation energies of these 2^- states are also within 0.6 MeV of the excitation energies predicted for two $T=1$, 2^- states by a shell-model calculation of Picklesimer and Walker.[14] In order to verify that the observed angular distributions for these transitions are consistent with $J^\pi=2^-$ assignments, we performed DWIA calculations with the code DWBA70 (Ref. 26) and the effective interaction of Love and Franey.[27] The nuclear structure for each of the 2^- states is assumed to be that of the shell-model calculation by Picklesimer and Walker. The shell-model calculation assumes a closed-shell configuration for ^{16}O and particle-hole states of $1\hbar\omega$ and $2\hbar\omega$ excitation in the final nucleus. Harmonic-oscillator eigenfunctions were assumed for the single-particle orbitals. The residual interaction assumed was a Serber-Yukawa potential adjusted to fit low-energy *n-p* scattering. In Table III, we list

TABLE III. Calculated particle-hole amplitudes.

J^π	E_x: ^{16}O (Calculated)[a] (MeV)	E_x: ^{16}F (Adjusted) (MeV)	E_x: ^{16}F (Observed) (MeV)	Particle-hole amplitudes[a]					
Odd parity				$1d_{3/2}$ $1p_{3/2}^{-1}$	$1d_{5/2}$ $1p_{1/2}^{-1}$	$1d_{5/2}$ $1p_{3/2}^{-1}$	$1d_{3/2}$ $1p_{1/2}^{-1}$	$2s_{1/2}$ $1p_{3/2}^{-1}$	
2^-	13.59	0.10	0.4	0.069	0.978	0.185	−0.022	0.063	
3^-	13.57	0.08	0.7	0.007	0.988	−0.152			
4^-	19.86	6.37	6.37			1.0			
2^-	20.96	7.47	7.6	−0.145	−0.162	0.650	−0.171	0.708	
1^-	23.26	9.77	9.4	0.181		0.882	0.329	0.261	
1^-	26.13	12.64	11.5	0.949		−0.051	−0.2773	−0.149	
Even parity				$2p_{3/2}$ $1p_{3/2}^{-1}$	$1f_{5/2}$ $1p_{3/2}^{-1}$	$1f_{5/2}$ $1p_{1/2}^{-1}$	$1f_{7/2}$ $1p_{3/2}^{-1}$	$1d_{5/2}$ $1s_{1/2}^{-1}$	$1f_{7/2}$ $1p_{1/2}^{-1}$
3^+	18.64	5.15	4.35	0.008	0.030	−0.012	0.111	0.039	0.993

[a]From Picklesimer and Walker.[14]

the particle-hole amplitudes for several states from the shell-model calculation of Picklesimer and Walker.[14] Note that in the assumed basis, the 4^- state is completely specified by the single $(\pi d_{5/2},\nu p_{3/2}^{-1})$ configuration. This 4^- state is predicted to be at $E_x=19.86$ MeV in ^{16}O, within 1 MeV of its observed excitation energy of 18.98 MeV. In Table III, we list the calculated excitation energies in ^{16}O as well as excitation energies in ^{16}F obtained by subtracting 13.49 MeV in order to place the 4^- state at its experimentally observed value of 6.37 MeV. This amounts to a shift of about 0.9 MeV of the calculated values (out of 15 to 20 MeV), plus the 12.6 MeV net displacement energy.

The DWIA calculations for the two 2^- states are compared in Figs. 10 and 11 with the measured angular distributions at 135 MeV. Both angular distributions show a large peak near 10° plus a smaller peak (or shoulder) near 35°. For both transitions, the large forward-angle peak is fit well by the DWIA calculations with the nuclear structure presented in Table III. For the transition to the state at $E_x=7.6$ MeV, the shoulder near 35° is largely fit also by the 2^- state calculation; whereas the angular distribution for the state at 0.40 MeV is severely underestimated in the region of the shoulder. Careful inspection of the energy spectra presented in Figs. 4 and 5 reveals that the state observed at 0.40 MeV near a scattering angle of 10° clearly moves at wider angles to a state at 0.70 MeV. (Recall that excitation energies in each spectrum are set relative to the ^{9}B ground state which was observed from the BeO target.) The state at 0.70 MeV is plausibly a 3^- state indicated in the compilation[7] with a tentative J^π assignment and predicted also by the shell-model calculation of Picklesimer and Walker to lie near the strong 2^- state. A $T=1$, 3^- state is known[7] in ^{16}O at $E_x=13.26$ MeV in good

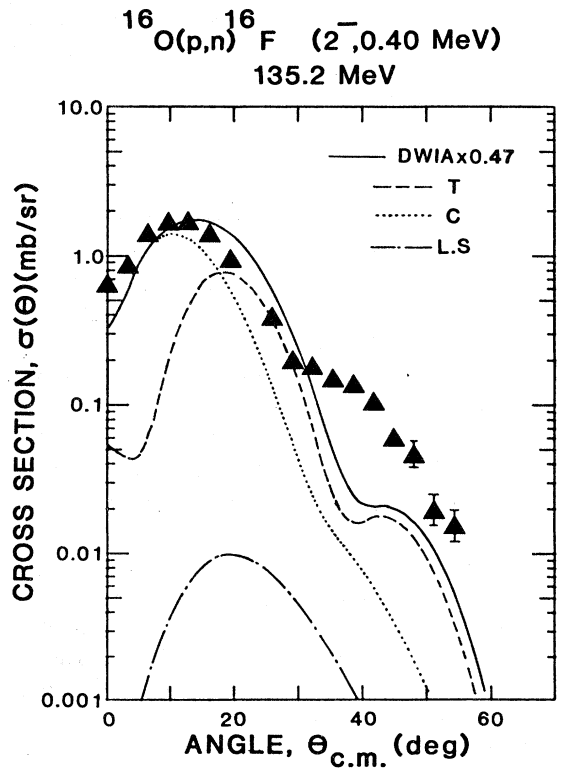

FIG. 10. Comparison of the measured angular distribution at 135 MeV for the transitions to the unresolved states at $E_x=0.40$ and 0.70 MeV with DWIA calculations for a 2^- state. (See discussion in the text.)

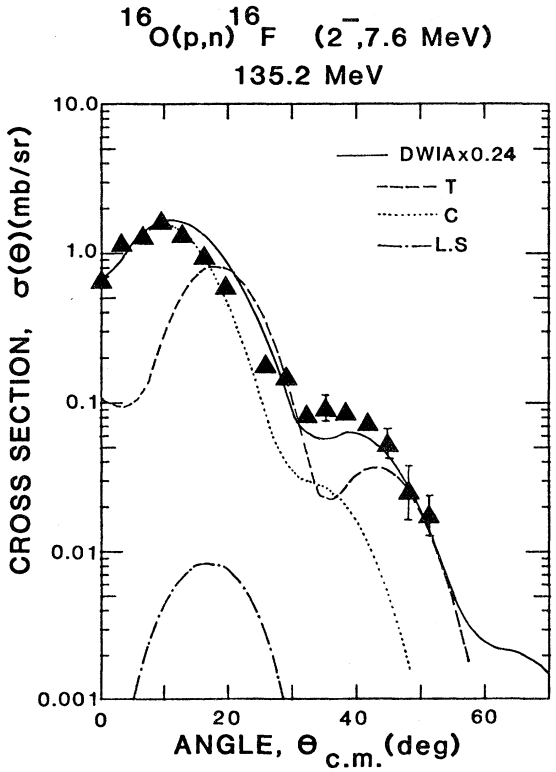

FIG. 11. Comparison of the measured angular distribution at 135 MeV for the transition to the state at $E_x=7.6$ MeV with DWIA calculations for a 2^- state. (See discussion in the text.)

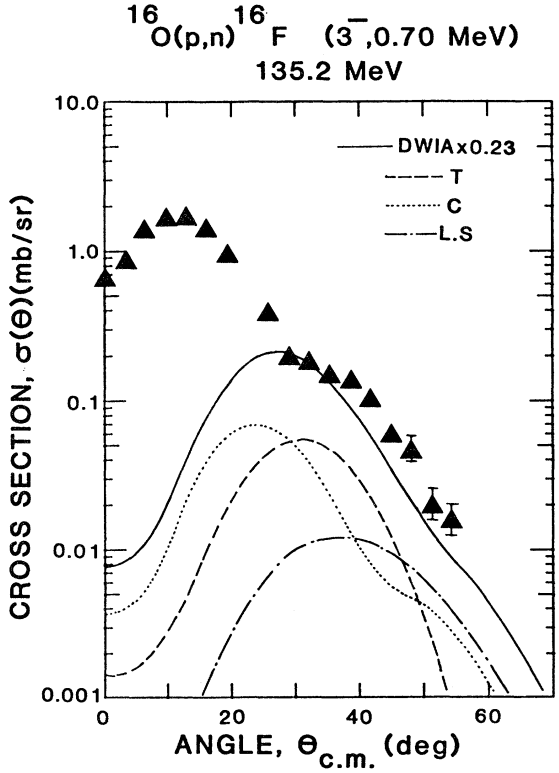

FIG. 12. Comparison of the measured angular distribution at 135 MeV for the transitions to the unresolved states at $E_x=0.40$ and 0.70 MeV with DWIA calculations for a 3^- state. (See discussion in the text.)

agreement with this state in ^{16}F still using a net displacement energy of 12.6 MeV. The shoulder of the angular distribution for the sum of these two states is fit reasonably well by the calculated angular distribution for the 3^- state as shown in Fig. 12. The structure for the 3^- state is taken also from the shell-model predictions presented in Table III.

The reason that the calculated angular distribution for the 2^- state at 7.6 MeV includes a strong contribution in the region of the shoulder at wider angles is that the predicted structure for this state indicates a large amplitude for the $(2s_{1/2},1p_{3/2}^{-1})$ particle-hole configuration. In contrast, the predicted structure for the lower-lying 2^- state indicates only a small amplitude for this configuration (see Table III). It is the radial distribution of the form factor for this transition which requires the larger angle in order to transfer the necessary angular momentum to excite a 2^- state. We note that the strong contribution of this configuration to the excitation of the 7.6 MeV 2^- state indicates that the (p,n) reaction at these energies is able to sample the entire volume of the target nucleus and is not confined to the surface region. This ability to interact throughout the nuclear volume is the result of the relatively long mean free path ($\sim$5 fm) for protons between 100 and 200 MeV, which is in contrast to the situation at lower energies.

In contrast to the 4^- state, which was dominated by the tensor term of the isovector effective interaction, we see from Figs. 10 and 11 that the excitation of both 2^- states is predicted to include approximately equal contributions from the central and tensor terms. The normalization factors required to make the DWIA calculations agree in magnitude with the observed cross sections are indicated to be 0.47 and 0.24 for the transitions to the 0.40 and 7.6 MeV states, respectively. These normalization factors are somewhat higher and lower, respectively, than the normalization factor required for the 4^- stretched state and may indicate that the simple nuclear structure assumed for these final states is approximately as accurate as the assumption that the 4^- state has a pure $(\pi d_{5/2},\nu p_{3/2}^{-1})$ configuration.

C. The states at 9.4 and 11.5 MeV

After the 4^- state at 6.37 MeV and the 2^- states at 0.40 and 7.6 MeV, the most strongly excited states are two relatively broad states at 9.4 and 11.5 MeV which, like the 2^- states, have angular distributions peaked near 10°. These two broad states are observed at excitation energies in good agreement with the known[7] $E1$ giant dipole resonance in ^{16}O, which has two major components at $E_x=22$ and 24 MeV. Using the net displacement energy of 12.6 MeV observed for the 4^- state (see discussion above), we show in Fig. 13 a comparison of the ^{16}O(γ,n)^{15}O excitation-energy spectrum[29] with our (p,n) spectrum at 11.8° and 100 MeV. The photoneutron cross section was arbitrarily normalized and added to an assumed flat background which corresponds to the nuclear continuum. The excitation-energy dependence of the two different measurements is clearly similar. Since these two resonances in ^{16}O have $J^\pi=1^-$, we tentatively identify these two states in ^{16}F to be 1^- also. To confirm this identification, we note that the shell-model predictions[14,30] indicate two strong 1^- states to be excited at $E_x=23.3$ and 26.1 MeV in ^{16}O in relatively good agreement with the known $E1$ resonance. The predicted structure for these two states is presented in Table III. Our DWIA calculations for these two transitions are compared in Figs. 14 and 15 with our measured angular distributions at 135 MeV. The calculated and measured angular distributions are in generally good agreement verifying that these transitions are $\Delta l=1$. Because these states align with known 1^- states in ^{16}O, and because the angular distributions agree with DWIA calculations for predicted 1^- states near these excitation energies, we conclude that these two broad states are predominantly $J^\pi=1^-$.

The DWIA calculations indicate that these transitions are dominated by the central term of the effective interaction. The relatively large increase of the total calculated cross section, including all terms coherently, would indicate that there is large constructive interference between the central and tensor terms for these transitions. Similar to the 2^- excitations, we see that normalization factors are required which are comparable to that needed for the 4^- state transition, indicating that these states are also reasonably described by the simple structure given in Table III.

Because of the dominance of spin-flip strength in the nucleon-nucleon effective interaction at these energies, one expects that the excitation of these states proceeds predominantly via $\Delta l=1$ plus spin flip. If this is the case, then one might also expect 2^- and 0^- states to be excited at this energy.

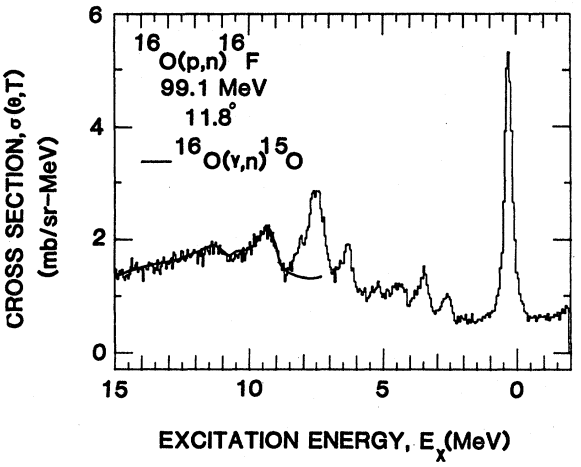

FIG. 13. Comparison of the excitation energy spectra for the ^{16}O(p,n)^{16}F reaction at 99.1 MeV with the known $E1$ giant resonance in ^{16}O excited by the photonuclear reaction ^{16}O(γ,n)^{15}O (from Ref. 8).

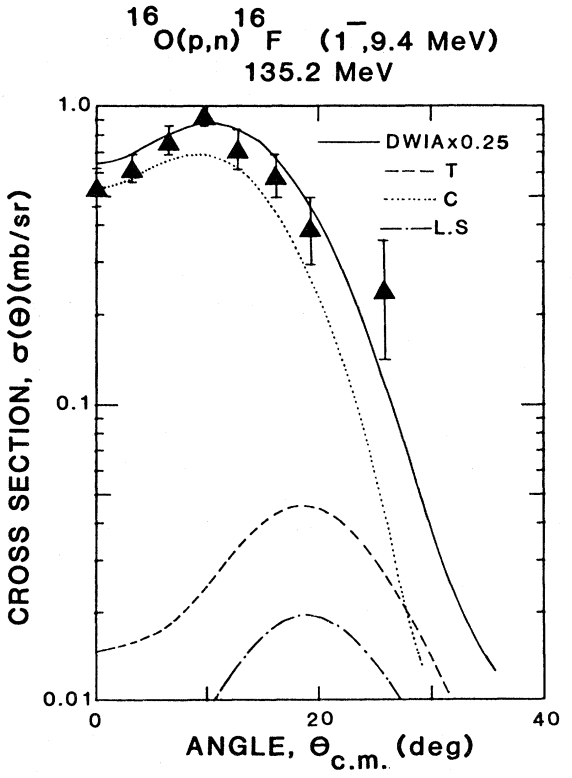

FIG. 14. Comparison of the measured angular distribution at 135 MeV for the transition to the broad state at $E_x=9.4$ MeV with DWIA calculations for a 1^- state. (See discussion in the text.)

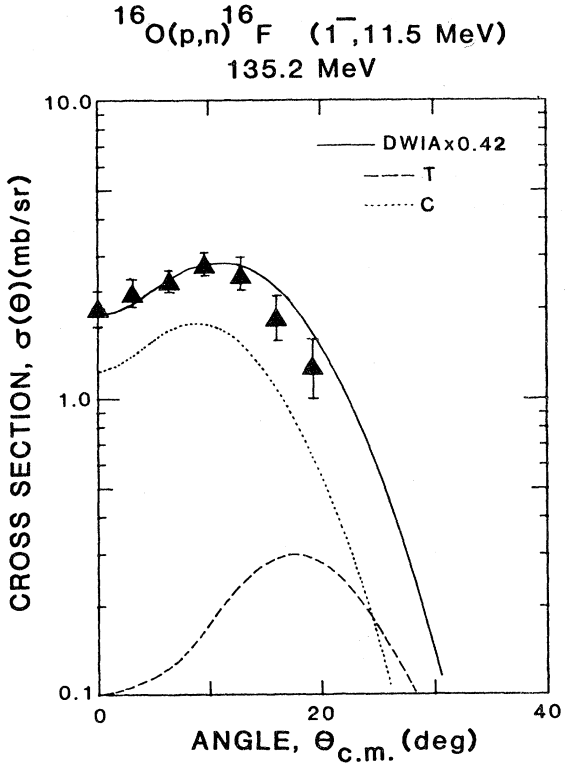

FIG. 15. Comparison of the measured angular distribution at 135 MeV for the transition to the broad state at $E_x=11.5$ MeV with DWIA calculations for a 1^- state. (See discussion in the text.)

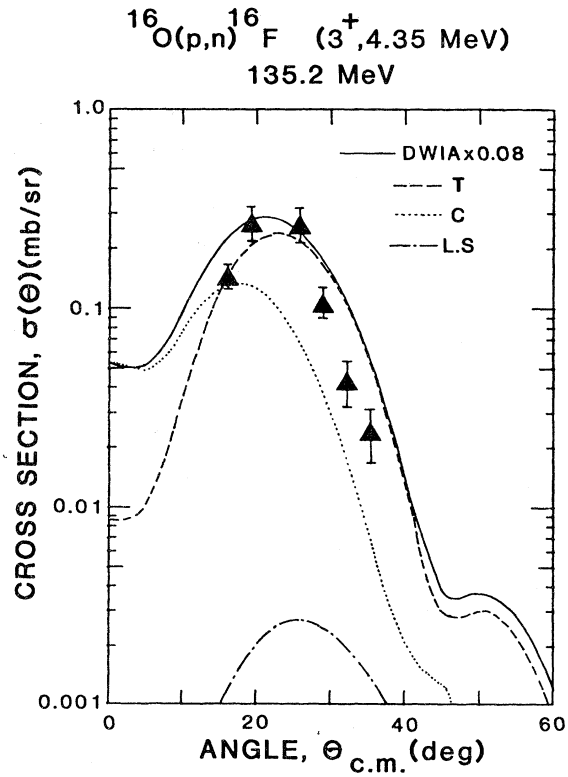

FIG. 16. Comparison of the measured angular distribution at 135 MeV for the transition to the state at $E_x=4.35$ MeV with DWIA calculations for a 3^+ state. (See discussion in the text.)

Indeed, the shell-model calculations of Picklesimer and Walker[14] (and also the earlier calculations of Moffa and Walker[30]) predict some 2^- and 0^- strength near these high-lying 1^- states; however, these 2^- and 0^- states are predicted to be less strongly excited than the 1^- states and to peak at larger momentum transfers. No strongly excited states are observed in this excitation energy region which peak at larger momentum transfer, so that we have no clear evidence for any 2^- or 0^- states in this region.

D. The 4.35 MeV state

A state is observed at 4.35 MeV with an angular distribution which peaks near 22°. Since this angular distribution indicates $\Delta l=2$, this state is plausibly a 3^+ state which would be the parent of a known 3^+ state in ^{16}O at 16.82 MeV (with no isospin assignment). These states align to within 150 keV still using the net displacement energy obtained from the 4^- state. A strong 3^+ state near this excitation energy is predicted by the shell-model calculation and its structure is listed in Table III. Figure 16 shows a comparison of our measured angular distribution for this transition compared to the DWIA calculation using the nuclear structure indicated in Table III. Although we note that the normalization factor needed to bring the calculations into agreement with the measurements is smaller here than for the previous cases, the good agreement in shape indicates that this state likely has $J^\pi=3^+$, as assumed. We *tentatively* assign this state $J^\pi=3^+$. The fact that the normalization factor required to make the DWIA calculation agree in magnitude with the measured cross sections is less than one-third of the factors required for the 4^- states, the 2^- states, or the 1^- states indicates that the structure of this state includes more complicated configurations than the simple one-particle, one-hole states assumed for the shell-model calculation.

E. The 3.75, 4.65, and 6.23 MeV states

In addition to the strongly excited states discussed above, we see also three weakly excited states with angular distributions peaked at 0°. These states necessarily involve $\Delta l=0$ transitions and are identified to be the analogs of the three $M1(1^+)$ states seen in ^{15}N($\vec{p},\gamma$)^{16}O by Snover *et al.*[13] and in ^{16}O(e,e') by Friebel *et al.*[10] The states in ^{16}O are seen at $E_x=16.22$, 17.14, and 18.80 MeV, which are all within 200 keV of the states in ^{16}F still using the net displacement energy of 12.6 MeV determined earlier. In the pure independent particle shell model, the doubly-closed shell nucleus ^{16}O has both the $p_{1/2}$ and $p_{3/2}$ subshells filled; therefore, low excitation-energy single-particle $M1$ transitions cannot occur and 1^+ excited states should not exist. Thus the observation of $M1$ type transitions provide direct evidence for ground-state correlations in ^{16}O. The sum of the 0° (p,n) cross sections to these three states has approximately the same ratio to the total $B(M1)$ strength[13] for the states in ^{16}O as does the 0° ^{12}C(p,n)^{12}N g.s. cross section to the $B(M1)$ value for the strongly excited 15.1 MeV state in ^{12}C (viz., $\sim$2 at 135 MeV). The total $B(M1)$ strength seen in these transitions is in reasonable agreement with a shell-model prediction by Arima and Strottman,[31] who calculate a 2p-2h intensity of 17% in the ^{16}O ground-state wave function. Their shell-model calculation also predicts an even larger amount of $M1$ strength at higher energies, fragmented over a number of levels. We see no obvious indication of such strength in ^{16}F from these measurements.

F. The 5.93 MeV state

A weakly excited state is seen at $E_x=5.93$ MeV with an angular distribution which peaks at the same angle as the angular distribution for the transition to the strongly excited 4^- state at 6.37 MeV. As seen in Fig. 7, the cross sections for the 5.93 MeV state are only about $\frac{1}{10}$ of the cross sections for the 6.37 MeV state. We identify this weakly excited state as the analog of a 4^- state seen in ^{16}O via the ^{16}O(e,e') and ^{13}C(^{6}Li,t) reactions.[8,11,32] This state is believed to be predominantly a multiparticle, multihole state which accounts for its weak excitation via the (p,n) reaction.

VI. DISCUSSION

We identify eleven states in ^{16}F whose analogs are known in ^{16}O. If, as discussed in Sec. V, we take the net displacement energy between states in ^{16}F and ^{16}O to be that observed for the strongly excited $T=1$, 4^- states at 6.37 MeV in ^{16}F and 18.98 MeV in ^{16}O, we find that all these states align to within $\pm$200 keV. In Fig. 17, we show the comparison of these eleven states in ^{16}O and ^{16}F. As indicated, the displacement forces the 4^- states to align, and then the others are allowed to come where they may. The overall agreement is seen to be excellent.

In Fig. 17, several of the states are labeled not only for spin and parity, but also by the multipolarity of a gamma transition to the ground state of ^{16}O. These multipolarities are often used to identify the states as an $M1$, $E1$, etc., type of excitation. Although we do not address the question of sum-rule strengths in this work, we note that several of the transitions reported here have cross sections which are a large fraction (typically 20–50%) of the DWIA calculations for these transitions using simple particle-hole shell-model wave functions as discussed in Sec. V. That the normalizations are less than 0.5 is likely due primarily to the neglect of multiparticle-multihole configurations in the shell-model description of the initial and final states; for example, Walker[9] notes that a reduction factor of 1.4 to 3 may be obtained for calculated cross sections for inelastic electron scattering excitation of

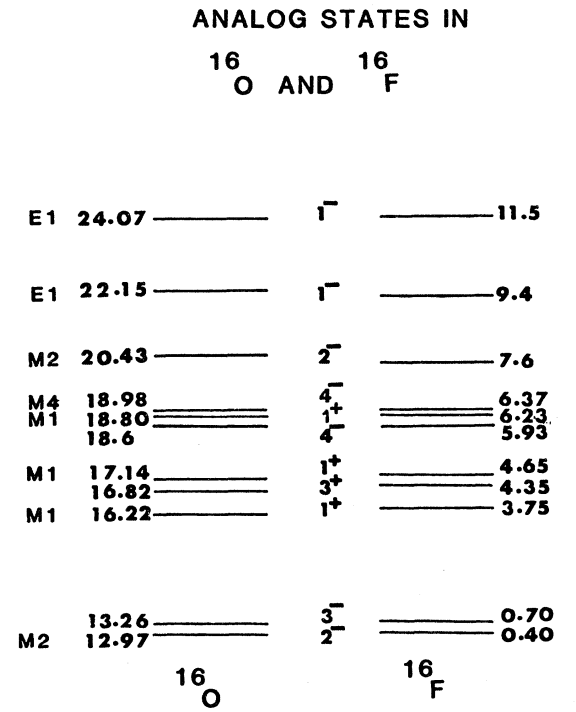

FIG. 17. Analog states in ^{16}O and ^{16}F. The excitation energies listed are in MeV.

the 2^- states in ^{16}O by assuming that the ground state of ^{16}O includes about a 25% 2p-2h component and including 3p-3h states in the final state configurations. Such reduction factors were reported[33,34] also in random-phase approximation calculations. Unfortunately, we are not able to incorporate such wave functions into the DWIA calculations presented here.

It is noteworthy that the shell-model predictions of Picklesimer and Walker,[14] as well as the earlier predictions of Moffa and Walker,[30] provide remarkable agreement with the measurements reported here. Both works combined the results of a shell-model calculation with a PWIA calculation in order to predict the excited state spectra. The shell-model calculations considered only one-particle, one-hole states of 1 and 2 $\hbar\omega$ excitations. The PWIA calculations used a nucleon-nucleon effective interaction[14] based on free nucleon-nucleon scattering parameters. The resulting predicted excited state spectra are compared with our measurements in Fig. 18. The predictions agree remarkably well with the measured spectra. The excitation energies of the several most strongly excited states are predicted correctly to within ~ 1 MeV (see Table III). The calculations predict the 2^- states near 0 and 8 MeV to be strongly excited, with a fairly strong 3^- state predicted to lie near the lower 2^- state. The calculations also correctly predict the strong 1^- states near 9.5 and 12 MeV, as well as the strong 4^- state near 6 MeV. Finally, the calculations also predict a 3^+ state to lie somewhat more than 1 MeV below the 4^- state in agreement with the measurements. No other strongly excited states are predicted and no other strongly excited states are observed. The other states we report here are the three 1^+ ($M1$) states and the 4^- state at 5.84 MeV. These four states are only weakly excited and require ground-state correlations or multiparticle, multihole configurations beyond the scope of the simple shell-model configurations. Finally, we note that the normalizations required for the DWIA calculations presented in Sec. V, which assume the nuclear structure obtained from these shell-model predictions, are between 0.23 and 0.47, except for the 3^+ state, which is 0.08. These normalizations are comparable to those required for (p,p') excitations of so-called stretched states as discussed by Lindgren *et al.*[35] Note also that similar normalization factors are required for the (e,e') excitation of stretched states, indicating that the normalization factors are required primarily to account for errors in the assumed nuclear structure and not in the reaction mechanism. The structure assumptions include a closed-shell configuration for the target nucleus and only one-particle, one-hole configurations for the final states. Clearly, both of these assumptions are simplifications and will tend to require normalization factors less than unity, as observed.

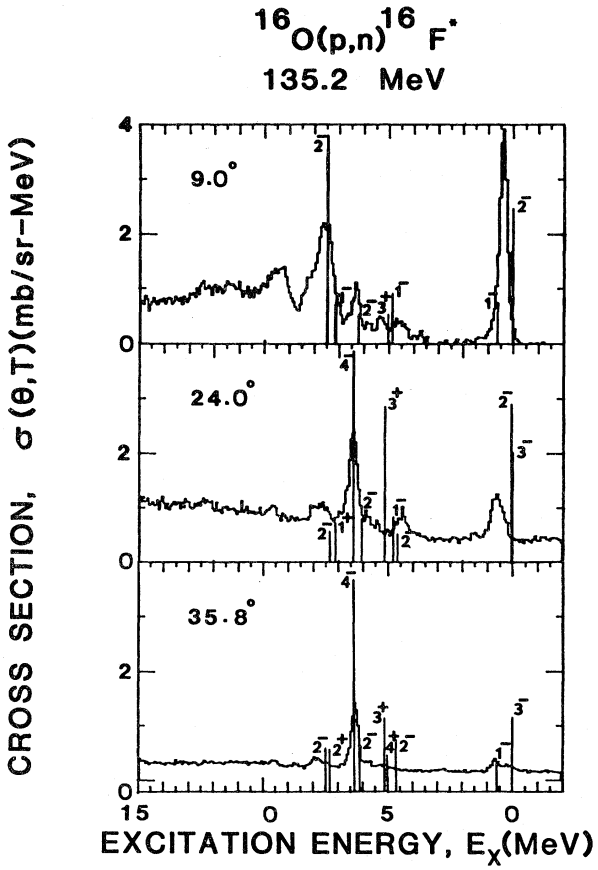

FIG. 18. Comparison of the PWIA calculations of Picklesimer and Walker (Ref. 14) with the measured neutron energy spectra reported here. The momentum transfers for the displayed angles nearly match the momentum transfers for the calculations.

Based on the good agreement we see for the states observed in ^{16}F with known analog states in ^{16}O, and with excitation energies and strengths predicted by shell-model calculations, we make the spin and parity assignments presented in Table IV. Shown also are the l transfers deduced by analysis of the measured angular distributions. Some of the previously known spin and parity assignments from the most recent compilation[17] are presented also.

TABLE IV. Energy levels of ^{16}F.

^{16}O$(p,n)^{16}$F: This work				Compilation		Assignment (this work)
E_x	Δl	π	J	E_x	J^π	J^π
				0	$(0)^-$	
				0.19	(1)	
0.40	1	−	0, 1, 2	0.42	$(2)^-$	2^-
0.70	3	−	2, 3, 4	0.72	$(3)^-$	3^-
3.75	0	+	0, 1	3.76	1^+	1^+
				3.87	$(2)^+$	
4.35	2	+	1, 2, 3	4.37		(3^+)
4.65	0	+	0, 1	4.65	1^+	1^+
				4.97		
5.26	1	−	0, 1, 2	5.26		
				5.39		
				5.45		
				5.53		
5.93	3	−	2, 3, 4	5.84		4^-
6.23	0	−	0, 1	6.23		1^+
6.37	3	−	2, 3, 4	6.37		4^-
				6.68		
				7.11		
7.6	1	−	0, 1, 2	7.73		2^-
9.4	1	−	0, 1, 2			1^-
11.5	1	−	0, 1, 2			1^-

VII. CONCLUSIONS

We measured neutron energy spectra for the ^{16}O$(p,n)^{16}$F reaction at 99.1 and 135.2 MeV and extracted angular distributions for eleven states in ^{16}F. By comparison of the measured excitation-energy spectra with known[7] analog states in ^{16}O and with shell-model calculations[14,30] for $T=1$ states in the $A=16$ system, we assigned spin and parity assignments for eight new levels of ^{16}F.

Important states observed in ^{16}F via the (p,n) reaction include two 2^- states at $E_x=0.40$ and 7.6 MeV, which are analogs of known 2^- states in ^{16}O at $E_x=12.97$ and 20.36 MeV, respectively. The 2^- state at higher excitation energy was identified in inelastic electron scattering as the magnetic quadrupole ($M2$) resonance. The (p,n) reaction strongly excites also the 4^- state at $E_x=6.37$ MeV which is dominated by the stretched $(\pi d_{5/2}, \nu p_{3/2}{}^{-1})$ configuration. The (p,n) excitation of this state in ^{16}F compares well with the ^{16}O(p,p') excitation of the analog 4^- state in ^{16}O (at $E_x=18.98$ MeV) verifying the dominant $T=1$ nature of this state and indicating that the states are good analogs. Strength observed at $E_x=9.4$ and 11.5 MeV in ^{16}F with $\Delta l=1$ angular distributions compare well with the known $E1$ giant dipole resonance in ^{16}O with major components at $E_x=22$ and 24 MeV. Three weakly excited states with $\Delta l=0$ angular distributions are observed at $E_x=3.75$, 4.65, and 6.23 MeV in good agreement with $M1$ states observed in ^{16}O. These states provide direct evidence for ground-state correlations in ^{16}O. Finally, we see a state weakly excited at $E_x=5.93$ MeV with a $\Delta l=3$ angular distribution which is likely the analog of a 4^- state observed in ^{16}O at $E_x=18.6$ via the ^{16}O$(e,e')^{16}$O and ^{13}C$(^6$Li$,t)^{16}$O reactions. This state is believed to be predominantly a multiparticle, multihole state which accounts for its weak excitation via the (p,n) reaction. Note that the same net displacement energy (12.6 ± 0.2 MeV) applies to all of the above comparisons of states in ^{16}F and ^{16}O. This consistent displacement reinforces the conclusion that these states are simply related.

These measurements strongly support the idea that (p,n) reactions at medium energies proceed primarily via a one-step process that preferentially excites the one-particle, one-hole component of nuclear states. The strongly excited states observed in these measurements are analogs of known $M1$, $M2$,

$M4$ or $E1$ resonances in ^{16}O. All of these states are believed to have large one-particle, one-hole components. Many of the dominant features seen in the (p,n) results are strikingly similar to those observed in backward-angle $^{16}O(e,e')$ measurements. That the (p,n) reaction at these energies predominantly excites states with simple nuclear configurations makes it a useful spectroscopic tool. Such spectroscopic studies are important because they often provide definitive isospin assignments, and because the residual nuclei reached via (p,n) reactions are generally not well understood in terms of spectroscopic information.

ACKNOWLEDGMENTS

We are grateful to the staff of the Indiana University Cyclotron Facility for their assistance during the running of this experiment and to Dr. P. C. Tandy and Dr. J. Kelly for conversations regarding this work. This work was supported in part by the National Science Foundation under Grants PHY79-07790, PHY79-23210, and PHY78-22774, and by the Department of Energy under Contract DE-AC-02-76 ERO-3069.

[1]C. D. Goodman, Bull. Am. Phys. Soc. 25, 732 (1980); C. D. Goodman, C. A. Goulding, M. B. Greenfield, J. Rapaport, D. E. Bainum, C. C. Foster, W. G. Love, and F. Petrovich, Phys. Rev. Lett. 44, 1755 (1980).

[2]F. Petrovich, W. G. Love, and R. J. McCarthy, Phys. Rev. C 21, 1718 (1980).

[3]B. D. Anderson, J. N. Knudson, P. C. Tandy, J. W. Watson, R. Madey, and C. C. Foster, Phys. Rev. Lett. 45, 699 (1980).

[4]C. Gaarde, J. S. Larsen, M. N. Harakeh, S. Y. Van der Werf, M. Igarashi, and A. Müller-Arnke, Nucl. Phys. A334, 248 (1980).

[5]G. F. Bertsch, Nucl. Phys. A354, 157c (1981). Reprinted in *Proceedings of the International Conference on Nuclear Physics, Berkeley, California,* edited by R. M. Diamond and J. O. Rasmussen (North-Holland, Amsterdam, 1981), p. 157c; G. Bertsch, D. Cha, and H. Toki, Phys. Rev. C 24, 533 (1981).

[6]J. W. Watson, M. Ahmad, B. D. Anderson, A. R. Baldwin, A. Fazely, P. C. Tandy, R. Madey, and C. C. Foster, Phys. Rev. C 23, 2373 (1981).

[7]F. Ajzenberg-Selove, Nucl. Phys. A281, 1 (1977); A375, 1 (1982).

[8]W. Bertozzi, Clinton P. Anderson Meson Physics Facility (LAMPF) Users Group Newslettter 13, 55 (1981).

[9]I. Sick, E. B. Hughes, T. W. Donnelly, J. D. Walecka, and G. E. Walker, Phys. Rev. Lett. 23, 1117 (1969).

[10]A. Friebel, H. -D. Gräf, W. Gross, W. Knüpfer, G. Küchler, G. Kühner, D. Meuer, S. Müller, A. Richter, E. Spamer, W. Steffen, W. Stock, and O. Titze, Proceedings of the International Conference on Nuclear Physics, Berkeley, California 1980, Lawrence Berkeley Laboratory Report LBL-11118, p. 233.

[11]C. Hyde, W. Bertozzi, T. Buti, M. Deady, W. Hersman, J. Kelly, S. Kowalski, R. Lourie, B. Pugh, C. P. Sargent, W. Turchinetz, B. Norum, B. L. Berman, M. V. Hynes, J. Lichtenstadt, F. Petrovich, D. Halderson, J. Karr, and W. G. Love, Bull. Am. Phys. Soc. 26, 27 (1981).

[12]R. S. Henderson, B. M. Spicer, I. D. Svalbe, V. C. Officer, G. G. Shute, D. W. Devins, D. L. Friesel, W. P. Jones, and A. C. Attard, Aust. J. Phys. 32, 411 (1979).

[13]K. A. Snover, in *Polarization Phenomena in Nuclear Physics-1980,* Proceedings of the 5th International Symposium on Polarization Phenomena in Nuclear Physics, edited by G. G. Ohlsen, R. E. Brown, N. Jarmie, M. W. McNaughton, and G. M. Hale (AIP, New York, 1981), p. 321; K. A. Snover, in *Neutron Capture Gamma Ray Spectroscopy,* edited by R. E. Chrien and W. R. Kane (Plenum, New York, 1979), p. 319; K. A. Snover, P. G. Ikossi, and T. A. Trainor, Phys. Rev. Lett. 43, 117 (1979).

[15]D. B. Holtkamp, W. J. Braithwaite, W. Cottingame, S. J. Greene, R. J. Joseph, C. Fred Moore, C. L. Morris, J. Piffaretti, E. R. Siciliano, H. A. Thiessen, and D. Dehnhard, Phys. Rev. Lett. 45, 420 (1980).

[16]C. D. Goodman, C. C. Foster, M. B. Greenfield, C. A. Goulding, D. A. Lind, and J. Rapaport, IEEE Trans. Nucl. Sci. NS-26, 2248 (1979).

[17]R. Madey, J. W. Watson, B. D. Anderson, A. R. Baldwin, M. Ahmad, R. Cecil, A. Fazely, and J. Knudson, Bull. Am. Phys. Soc. 25, 539 (1980).

[18]B. D. Anderson, J. N. Knudson, and R. Madey, Nucl. Instrum. Methods 169, 153 (1980).

[19]R. Madey, F. M. Waterman, and A. R. Baldwin, Nucl. Instrum. Methods 133, 61 (1976).

[20]A. R. Baldwin and R. Madey, Nucl. Instrum. Methods 171, 149 (1980).

[21]A. R. Baldwin and R. Madey, Nucl. Instrum. Methods (to be published).

[22]P. R. Bevington, K. G. Kibler, and B. D. Anderson, Case Western Reserve University Report No. COO-1573-63, 1969 (unpublished); P. R. Bevington, *Data Reduction and Error Analysis for the Physical Sciences* (McGraw-Hill, New York, 1969), p. 237.

[23]R. Cecil, B. D. Anderson, and R. Madey, Nucl. Instrum. Methods 161, 439 (1979).

[24]F. S. Crawford, Jr., Rev. Sci. Instrum. 24, 552 (1953).

[25]D. J. Hughes and R. B. Schwartz, Brookhaven National Laboratory Report BNL 325, 1958 (unpublished).
[26]J. Raynal and R. Schaeffer, computer code DWBA70. The version we used was supplied to us by W. G. Love.
[27]W. G. Love and M. A. Franey, Phys. Rev. C 24, 1073 (1981).
[28]J. R. Comfort and B. C. Karp, Rev. C 21, 2162 (1980).
[29]R. L. Bramblett, J. T. Caldwell, R. R. Harvey, and S. C. Fultz, Phys. Rev. 133, B869 (1964).
[30]P. J. Moffa and G. E. Walker, Nucl. Phys. A222, 140 (1974).
[31]A. Arima and D. Strottman, Phys. Lett. 96B, 23 (1980).
[32]H. Nann, A. D. Bacher, G. T. Emory, C. C. Foster, D. L. Friesel, W. P. Jones, and C. Olmer, Indiana University Cyclotron Facility Scientific and Technical Report, 1979, p. 104.
[33]V. Gillet and M. A. Melkanoff, Phys. Rev. 133, B1190 (1964).
[34]A. Fujii, M. Morita, and H. Ohtsuba, Prog. Theor. Phys. Suppl. Extra Number, 303 (1968).
[35]R. A. Lindgren, W. J. Gerace, A. D. Bacher, W. G. Love, and F. Petrovich, Phys. Rev. Lett. 42, 1524 (1979).